Jpn. J. Appl. Phys. Vol. 40 (2001) pp. 5920–5924
Part 1, No. 10, October 2001

Interfaces of Photonic Crystals for High Efficiency Light Transmission

Toshihiko BABA and Daisuke OHSAKI

Yokohama National University, Division of Electrical and Computer Engineering, 79-5 Tokiwadai, Hodogayaku, Yokohama 240-8501, Japan

(Received May 22, 2001; accepted for publication July 12, 2001)

Input and output interfaces of photonic crystals are discussed for high efficiency transmission of light. The discussion focuses on the frequency range higher than the photonic bandgap, at which a small group velocity of light, the superprism effect, the strong structural birefringence and the negative refractive index effect are expected. The two-dimensional photonic crystal of triangular lattice airholes in a high-refractive-index dielectric medium is assumed as the fundamental model. The finite difference time domain simulation shows that two types of interfaces improve the transmission efficiency. One is composed of small airholes and the other is composed of projected airholes. In particular, the latter generates a wide transmission band of ~ 0.1 times the center frequency with the maximum efficiency of -0.01 dB against the normal or slightly inclined incidence of the TE-polarized wave.

KEYWORDS: photonic crystal, photonic band, superprism, FDTD

1. Introduction

Photonic crystals (PCs), i.e., multidimensional periodic structures, have attracted much attention due to their novel concept of optics combined with solid-state physics and their crystallography, and also due to the potential of applications in various devices in next-era optoelectronic systems. As applications, their use in defect lasers and waveguides is studied by many groups. Since they utilize the forbidden photonic bandgap (PBG), we can call them reflection-type devices. Also, there are some reports on transmission-type devices, which utilize peculiar dispersion characteristics of allowed bands above the PBG, *e.g.*, a narrow band filter, a dispersion compensator and an optical deflector based on the superprism effect,[1–3] nonlinear devices based on the small group velocity,[3–9] a polarization filter based on the structural birefringence,[10] and an image processor based on the negative refractive index effect.[11] However, discussions have mainly focused on the functions of PCs. Quantitative discussions on light transmission efficiency are limited, although it is one of the most fundamental specifications of these devices. There are two major losses which degrade the transmission efficiency, i.e., the diffraction loss inside the PC and the reflection loss at input and output ends of the PC. The former is an essential problem related to the dispersion characteristics of photonic bands.[1] It is negligible when the PC is sufficiently large, or it may be reduced by using the collimating effect with a flat equi-frequency curve in a dispersion surface.[12] On the other hand, there are no discussions on the reduction of reflection loss except for a brief comment.[13]

In this paper, we discuss the reduction in reflection loss at the ends of a two-dimensional (2-D) PC, through the finite difference time domain (FDTD) calculation. As a fundamental model, we employ one of the most popular structures studied by many groups, i.e., PCs composed of triangular lattice airholes in a high-refractive-index dielectric medium. First, we show the relationship between photonic bands and transmission spectra, and discuss the mechanism of reflection loss. Then, we discuss two types of input and output interfaces. One is composed of small airholes and the other is composed of projected airholes. We show that the latter is effective for reducing the reflection loss and improving the transmission efficiency in a meaningful wide spectral range. We show the dependence of this effect on the polarization and angle of incident waves and discuss its possibility for practical use.

2. Condition of FDTD Calculation

For all calculations in this paper, we assume 2-D models which are infinite in the third dimension. The fundamental model of the PC and the corresponding Brillouin zone are shown in Fig. 1. As examples, the refractive index of the background dielectric medium is assumed to be 3.065 for the transverse-electric (TE) polarization with the electric field $\boldsymbol{E}$ parallel to the 2-D plane, and 2.635 for the transverse-magnetic (TM) polarization with $\boldsymbol{E}$ perpendicular to the 2-D plane. These are modal indexes of an airbridge PC slab with a material index of 3.5 and thickness of 0.32 μm at a wavelength λ of 1.55 μm.[14] Recently, such PC slabs have become very popular in studies of PC waveguides and photonic circuits, because of their easy fabrication process. By assuming the above indexes, we expect that the calculated results in this study can be used in other experiments and discussions, not only on deep 2-D PCs but also on PC slabs. Strictly speaking, PC slabs require a full 3-D calculation. Therefore, a quanti-

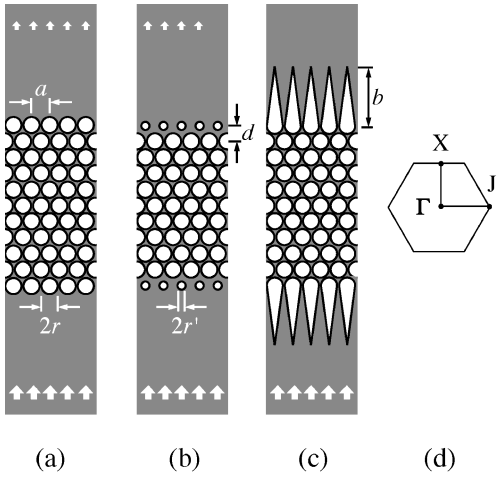

Fig. 1. Schematic of 2-D PCs of triangular lattice circular airholes in a dielectric medium. (a) Fundamental structure A composed of 9 rows of airholes, (b) structure B with small airhole interfaces, and (c) structure C with projected airhole interfaces. (d) shows the Brillouin zone of a PC.

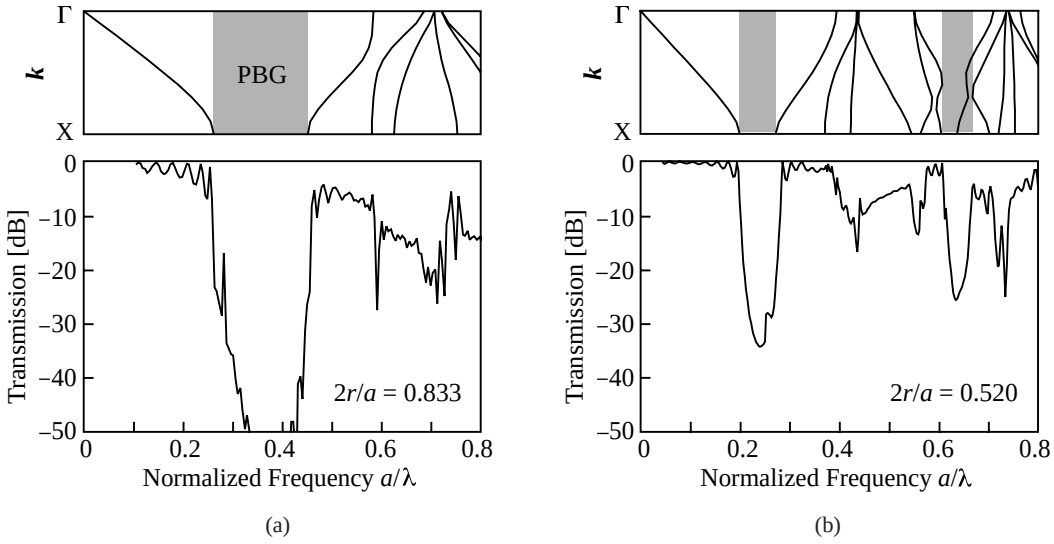

Fig. 2. Photonic bands and transmission spectra for TE-polarized wave in structure A: (a) $2r/a = 0.833$ and (b) 0.520.

tative discussion on PC slabs is difficult with the 2-D calculation. However, the qualitative discussion is possible, since projected 3-D bands for PC slabs[15] are roughly evaluated by 2-D bands with the modal index approximation.

In FDTD calculations of transmission spectra, we first assume that the PC is infinitely wide and its front and back ends orient toward the Γ–J direction in the Brillouin zone. These assumptions allows us to eliminate edge effects in a finite-width PC and complicated scattering at uneven ends orienting toward the Γ–X direction, respectively, thus simplifying the problem. Nine unit cells are assumed to be the length of the PC in the Γ–X direction. Except for some calculations shown in §5, the incident wave is an infinitely wide, TE-polarized plane wave propagating along the Γ–X direction. To simulate this condition, the calculation area is reduced to the unit cell in the Γ–J direction by applying the periodic boundary condition. In the FDTD algorithm, 60 square Yee cells divide the calculation area in this direction. The front and back ends of the analysis area are terminated by Berenger's perfect matched layer absorbing condition. For these ends, the reflection loss of more than 140 dB is confirmed against the incident wave. The incident wave is excited for the field perpendicular to the 2-D plane on a horizontal line close to the front end with the Gaussian time function. Poynting powers of incident and reflected waves and that of the transmitted wave are measured on other horizontal lines close to the front and back ends, respectively. The transmission spectrum is evaluated from the ratio of the transmitted power to the incident power after the fast Fourier transform.

3. Transmission Spectra and Photonic Bands

The correspondence of transmission spectra using the FDTD method and photonic bands using the plane-wave expansion method[16] is demonstrated in Fig. 2. Here, $2r/a = 0.833$ and 0.520 are assumed, where $2r$ is the air-hole diameter and a is the pitch of the triangular lattice. To minimize the digitizing error in the FDTD algorithm, the $2r$ assumed in the FDTD is optimized so that the total area of Yee cells in one airhole is closest to the target area πr^2 assumed in the plane wave expansion method. In Figs. 2(a) and 2(b), the frequency range exhibiting very low transmission corresponds to the PBG. Almost perfect transmission with some Fabry–Perot resonance is observed at lower frequencies than the PBG. On the other hand, spectra are much more complicated at higher frequencies due to the strongly modulated photonic bands exhibiting small group velocities, ministopbands and uncoupled modes. For larger airholes, the transmission efficiency at these frequencies is less than −5 dB. Figure 3(a) shows the magnetic field distribution of light. Here, we assume the finite-width PC and the calculation area absolutely terminated by the absorbing condition in order to gain a better understanding of the field profile inside

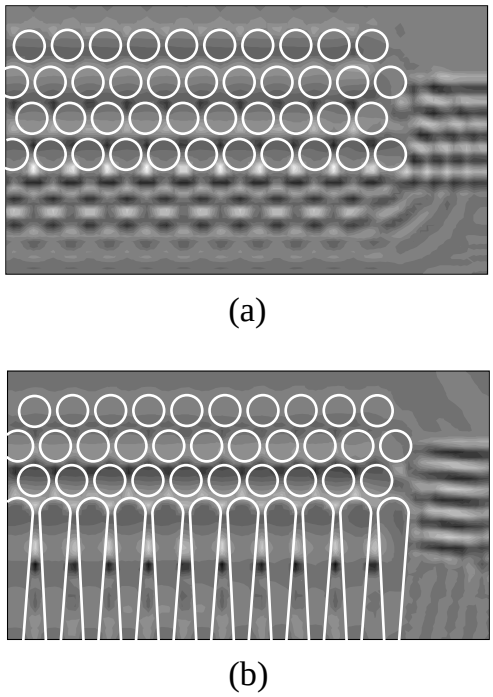

Fig. 3. Distribution of TE-polarized Gaussian-pulsed wave (magnetic field normal to the 2-D plane) with center normalized frequency $a/\lambda = 0.665$ in structures A (a) and C (b) with $2r/a = 0.833$. For structure C, $b/2r = 8$ is assumed.

and outside the PC and of the additional edge effects at the PC edge. The Bloch wave inside the PC at these frequencies spatially oscillates in both Γ–X and Γ–J directions. Therefore, the coupling of the incident plane wave to the Bloch wave is essentially inefficient. Uncoupled waves are converted to reflected waves and scattered in various directions that satisfy the Bragg diffraction condition. For smaller airholes, the transmission efficiency is improved due to the shallow oscillation depth of the field in the Γ–J direction and relatively slow transition from the incident plane wave to the Bloch wave in the crystal. A similar improvement is expected for a lower index background medium. However, this weakens the interaction between the PC and the incident wave, and essentially increases the required length of the target PC device. Therefore, such simple designs are not acceptable, and some additional modification of the structure is necessary, if one aims to achieve a small device.

Regarding modifications, we investigate two types of input and output interfaces. One is structure B with small airholes, as shown in Fig. 1(b). It effectively realizes the intermediate refractive index layer between the PC and the background medium. The other is structure C with projected airholes, as shown in Fig. 1(c). It realizes the adiabatic transition of light waves in the gradually transformed structure.

4. Small Airhole Interface

In general, a simple dielectric interface between two media with refractive indexes n_1 and n_2 is made antireflective by inserting another medium with an intermediate index of $\sqrt{n_1 n_2}$ and an odd-multiple thickness of the quarter-wavelength in the medium. The small airhole interface has a similar effect. A line of small airholes has an effective intermediate index between the effective index of the PC and the background index. Figure 4(a) shows transmission spectra for a PC with the interfaces at both front and back ends, a PC with the interface at only the front end, and the PC without the interface. Evidently, a pair of interfaces improves the transmission efficiency. In particular, at $a/\lambda = 0.693$, the maximum efficiency is over -1 dB. Figure 4(b) shows the dependence of the efficiency on the normalized radius of the small airholes r'/r. Maximum efficiency is achieved at $r'/r = 0.59$. This optimum radius is explained by the intermediate index, as mentioned above. The effective index of the PC, which is estimated from the slope of the lowest photonic band at the low frequency limit, is 1.57, while that of a PC composed of the small airholes is 2.17. The latter is equal to the intermediate index between the effective index of the PC and the background index of 3.065. However, as observed in Fig. 4(a), the high transmission range is too narrow to make it applicable to some practical devices. In addition, the spectral behavior is so complicated that further discussion on physical phenomena in this structure may be difficult.

5. Projected Airhole Interface

Regarding antireflective structures, various projected interfaces have been studied in the fields of radio waves and optics. In particular, a dielectric surface with many random projections smaller than the optical diffraction limit acts as a wideband antireflection coating. For PCs, on the other hand, structure C with periodic projections is more reasonable to investigate, since the transmitted wave in the PC is not a free traveling wave but a set of Bloch waves.

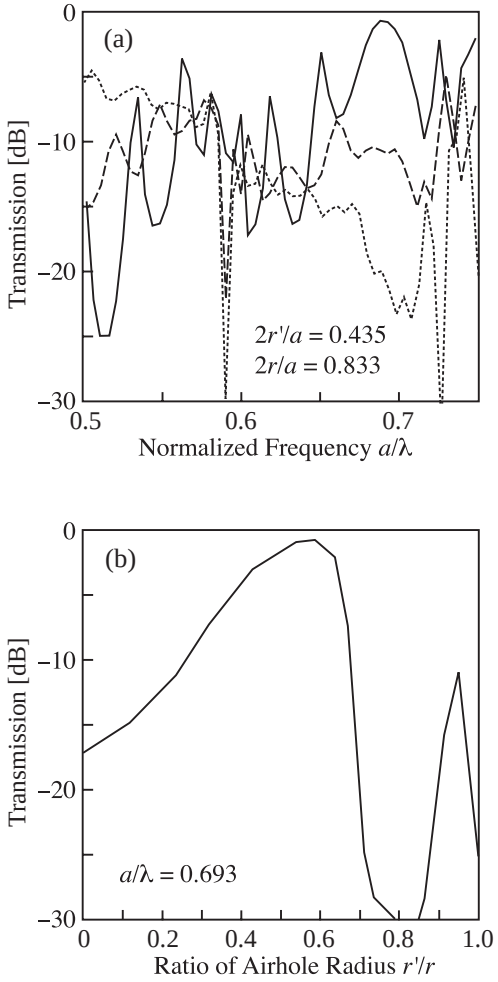

Fig. 4. Transmission characteristics of TE-polarized wave in PCs with and without small airhole interface. $2r/a = 0.833$. (a) Transmission spectra. Solid and dotted lines indicate structures B and A, respectively. The dashed line indicates the intermediate structure in which only the input end has the small airhole interface. For small airholes, $2r'/a = 0.435$ is assumed. (b) Dependence of the maximum transmission efficiency on normalized radius of small airholes at $a/\lambda = 0.693$.

The transmission spectrum is shown in Fig. 5(a), where the projection length b normalized by the airhole diameter $2r$ is assumed to be 3. In a wide frequency range of $a/\lambda = 0.59$–0.67, the transmission efficiency is increased to > -0.5 dB. Maximum efficiency reaches -0.01 dB. The antireflection effect is clearly observed through the comparison of three cases similar to that in Fig. 4(a). The frequency range is shifted by changing the projection length. Similarly, the efficiency at a specified frequency depends on the projection length, as shown in Fig. 5(b). The efficiency exhibits periodic characteristics with the change in the projection length. This can be understood from the field profile, as shown in Fig. 3(b). The phase difference of the incident wave occurs between inside and outside the projected airholes. When the phase shift matches that of the Bloch wave inside the PC, the transmission efficiency achieves a maximum. This is the reason of the periodic characteristic against the projection length and its frequency dependence. When the normalized projection length is 0.5–1, each projection has 45°–60° boundaries. They act as corner mirrors which significantly suppress the

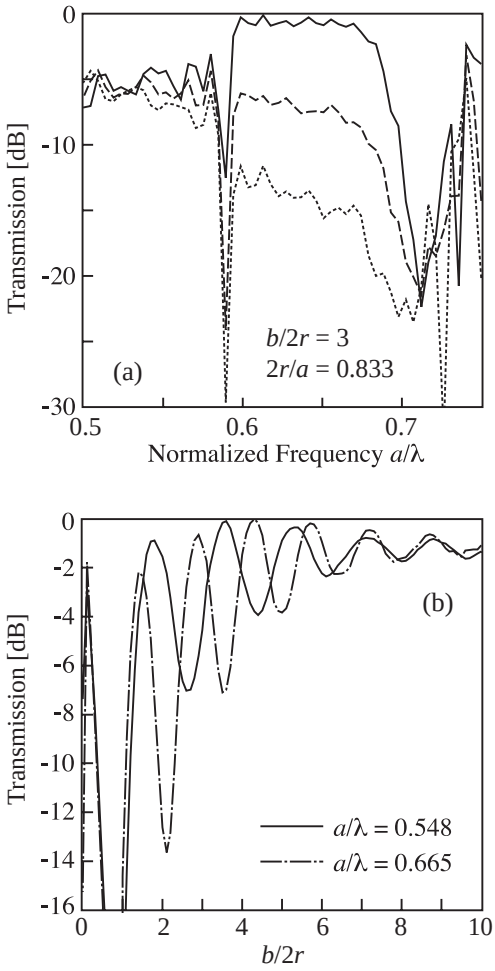

Fig. 5. Transmission characteristics of TE-polarized wave in PCs with and without projected airhole interface. $2r/a = 0.833$. (a) Transmission spectra. Solid and dotted lines indicate structures C and A, respectively. The dashed line indicates the intermediate structure in which only the input end has the projected airhole interface. For projected airholes, $b/2r = 3$ is assumed. (b) Dependence of transmission efficiency on the normalized length of projected airholes. Solid line indicates $a/\lambda = 0.548$ and dash-dot line 0.665.

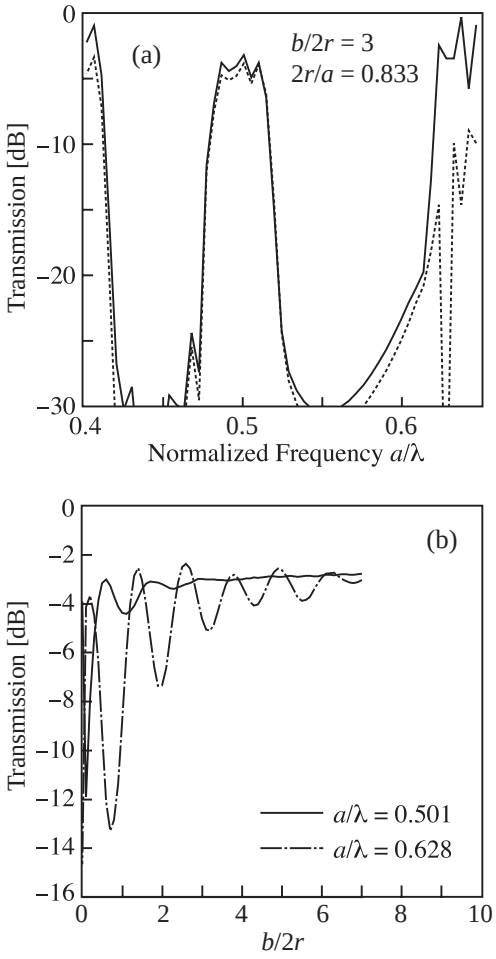

Fig. 6. Transmission characteristics of TM-polarized wave with and without projected airhole interfaces. $2r/a = 0.833$. (a) Transmission spectra. Solid and dotted lines indicate structures C and A, respectively. For projected airholes, $b/2r = 3$ is assumed. (b) Dependence of transmission efficiency on the normalized length of projected airholes. Solid line indicates $a/\lambda = 0.501$ and dash-dot line 0.628.

transmission. Figure 5(b) indicates that the optimum $b/2r$ is nearly 4. However, this is not an essential length, but one originating from the digitized model of the FDTD calculation. At this $b/2r$ or its odd multiple, the reflection at small steps of the projected airholes expressed by Yee cells is negated by each other. When $b/2r \sim 8$, the maximum transmission efficiency in Fig. 5(b) is limited to around -1 dB due to the opposite condition. Actually, however, this length will also achieve a high efficiency close to 0 dB.

Thus far, TE polarization has been assumed. Let us check transmission characteristics for TM polarization. Figure 6(a) shows transmission spectra for PCs with and without projected airhole interfaces. The spectral shapes are very different from those for TE polarization, since there are two PBGs. Even at frequencies outside the PBGs, the improvement of the transmission efficiency by the interfaces is not evident. The dependence of the efficiency on the normalized projection length is shown in Fig. 6(b). Maximum efficiency is limited to -3 dB. This low value is due not to the digitized model, but to the essential reflection of the structure. This reflection cannot easily be explained quantitatively. We consider that the TM-polarized wave undergoes large Fresnel reflection at the inclined boundaries of the projected airholes, while the existence of the Brewstar angle reduces this reflection for the TE-polarization.

Figure 7 shows the dependence of the maximum transmission efficiency for TE polarization on the angle of the incident wave measured from the Γ–X direction. Here, we used a PC model with finite width. Even when the width is as large as 50 unit cells, the incident wave suffers strong diffraction in the Γ–J direction by the small group velocity effect and partly by the superprism effect. This results in an excess loss of more than 3 dB. To investigate the angle dependence separately from the diffraction effect, results in Fig. 7 are plotted as the change of the efficiency against the normal incidence. Although it is not explicitly displayed in Fig. 7, the absolute value of the efficiency is much higher in the PC with the projected airhole interface than without the interface. However, Fig. 7 indicates that the efficiency is degraded more sensitively when the PC has the interface. Efficiency over -1 dB is only maintained for an inclination angle of less than 3°.

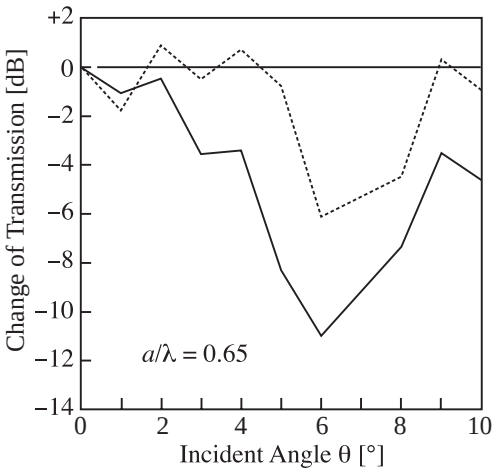

Fig. 7. Change of transmission efficiency with inclination angle θ of TE-polarized incident wave. $2r/a = 0.833$ and $a/\lambda = 0.650$ are assumed.

6. Conclusion

The FDTD simulation shows that the small airhole interface and the projected airhole interface improve the transmission efficiency at a frequency range higher than the PBG in a triangular lattice airhole PC. In particular, the latter allows a high transmission efficiency of a maximum of -0.01 dB within the frequency range of 0.1 times the center frequency. Such efficiency is sufficiently high and such a frequency range is sufficiently wide, when phenomena such as the small group velocity and superprism effect of the PC are used in actual applications. This interface is only effective for TE polarization with an inclination angle of less than 3°. Still, we believe that this interface is practicable, since most of the functional effects in photonic crystals at the higher frequency range are expected for normal or slightly inclined incidence of the TE-polarized wave.

Acknowledgements

The authors would like to thank Professor Y. Kokubun, Yokohama National University, and Professor K. Iga and Professor F. Koyama, Tokyo Institute of Technology, for helpful suggestions. This work was supported by Grant-in-Aid #10210203 from the Ministry of Education, Culture, Sports, Science and Technology and by CREST #530-13 of Japan Science and Technology Corporation.

1) H. Kosaka, T. Kawashima, A. Tomita, M. Notomi, T. Tamamura, T. Sato and S. Kawakami: Phys. Rev. B **58** (1998) 10096.
2) H. Kosaka, T. Kawashima, A. Tomita, M. Notomi, T. Tamamura, T. Sato and S. Kawakami: Appl. Phys. Lett. **74** (1999) 1370.
3) T. Baba, D. Ohsaki, T. Iwai and M. Nakamura: Proc. Conf. Laser and Electro-Optics Pacific Rim, 2001, TuA3-5.
4) K. Sakoda and K. Ohtaka: Phys. Rev. B **54** (1996) 5742.
5) J. Martorell, R. Vilaseca and R. Corbalan: Appl. Phys. Lett. **70** (1997) 702.
6) S. A. Asher, S. Y. Chang, S. Jagannsthan, R. Kesavamoorthy, T. India and G. Pan: US Patent 999487 (1992).
7) R. J. Spry and T. City: US Patent 925858 (1986).
8) A. Figotin, Y. A. Godin and I. Vitebsky: Phys. Rev. B **57** (1998) 2841.
9) T. Baba, T. Yonehana and D. Ohsaki: Proc. Int. Workshop Femtosecond Technology, 2000, FB-7.
10) Y. Ohtera, T. Sato, T. Kawashima, T. Tamamura and S. Kawakami: Electron. Lett. **35** (1999) 1271.
11) M. Notomi: Phys. Rev. B **62** (2000) 10696.
12) H. Kosaka, T. Kawashima, A. Tomita, M. Notomi, T. Tamamura, T. Sato and S. Kawakami: Appl. Phys. Lett. **74** (1999) 1212.
13) S. Kawakami, Y. Ohtera and T. Kawashima: Oyo Buturi **68** (1999) 1335 [in Japanese].
14) T. Baba, N. Fukaya and A. Motegi: Electron. Lett. **37** (2001) 761.
15) S. G. Johnson, S. Fan, P. R. Villeneuve and J. D. Joannopoulos: Phys. Rev. B **60** (1999) 5751.
16) K. M. Ho, C. T. Chan and C. M. Soukoulis: Phys. Rev. Lett. **65** (1990) 3152.